Oxygen mobility in yttrium hydride films studied by isotopic labelling

Dmitrii Moldarev[1,2*], *Camille* Aracheloff[1], *Marcos V.* Moro[1], *Eduardo* Pitthan[1], *Max* Wolff[1] and *Daniel* Primetzhofer[1]

[1]Department of Physics and Astronomy, Uppsala University, Box 516, 751 20 Uppsala, Sweden
[2]Department of Material Science, Moscow Engineering Physics Institute, 115409, Moscow, Russia

Abstract. The photochromic properties of oxygen-containing yttrium hydride thin films are directly dependent on the oxygen concentration in the material. We use $^{16}O/^{18}O$ labelling to study oxidation of YH_2 films. Oxygen penetrates the film through grain boundaries and intercolumnar voids oxidising the whole film thickness, without pronounced surface oxidation or self-passivation. Once oxidised, the mobility of oxygen in the films is low and no detectable changes in chemical composition of ^{18}O-labeled YHO films is found under illumination.

1 Introduction

The nearly exponential rise of the global energy demand over the last decades necessitates the development of sustainable technologies [1]. Smart windows based on photochromic materials represent a promising technology to save energy as they enable passive control of heat and light flow between buildings and the environment. Oxygen-containing yttrium hydride (YHO) [2] and some other oxygen-containing rare-earth metal hydrides (REMHO) [3], [4] in general, may show reversible photochromism – a modulation of the optical transmittance under illumination. The effect is observed at room temperature and ambient conditions and accompanied by a persistent photoconductivity [5]. Unlike their transition metal oxide counterparts, photodarkening in REMHO happens uniformly over the visible range without pronounced absorption bands [6], [7]. In practice, it implies that films do not change their color but transparency, which makes this material a good candidate for application in smart windows.

Photochromic YHO thin films are commonly produced in a two-step process. In the first step, a thin film of yttrium dihydride (YH_2) is deposited on a substrate using either reactive magnetron sputtering [8] or e^--beam evaporation [9]. After deposition the film is exposed to oxygen, often by venting the sputtering chamber, and oxidized. Thus, the opaque metal hydride turns into a transparent and photochromic oxygen containing metal hydride [10]. The amount of oxygen incorporated into the film at the final step determines the photochromic behavior of YHO. Photochromism is found for oxygen to yttrium ratios between 0.5 and 1.5, with the oxygen replacing hydrogen atoms under oxidation. Moreover, a general trend of decreasing photochromic activity with increasing oxygen concentration is reported [3], [11].

* Corresponding author: dmitry.moldarev@physics.uu.se

A comprehensive understanding of the oxidation process of YH_2 is vital for controlled synthesis of photochromic films with tailored properties.

Despite the high relevance of YHO for potential technological applications, the nature of its photochromic effect remains under debate. In Ref. [12], a reversible lattice contraction under illumination was reported, suggesting atomic rearrangements being related to the photodarkening. Positron annihilation and muon spin relaxation experiments suggest anion transport in connection with the photochromic effect [13], [14]. Along this line Baba et al. propose a light-induced oxygen breathing during photodarkening and bleaching [15]. However, experiments in high vacuum [16], [17] and with films encapsulated by diffusion barriers [18] show a persistent photochromic effect without the need of material exchange with the environment. Material transport, oxygen or hydrogen, within the film may still be possible. Recent findings suggest that photochromic films are composed of two phases [19] with a hydrogen rich columnar structure separated by oxygen rich regions. Material transport between these two phases may have the potential to explain the photochromism.

In this work, we study the oxidation of YH_2 and oxygen mobility in YHO. We use bilayer structures of YH_2/YHO and show that oxygen does not migrate from the oxidized layer into the dihydride. To trace the oxygen mobility and exchange with the environment we partially oxidize films in $^{18}O_2$ enriched atmosphere and study the redistribution under exposure to air. Finally, we investigate light-induced changes in chemical composition of YHO films and find no long-range oxygen diffusion.

2 Experimental details

2.1 *In-situ* experiment

The experiments were conducted in the scattering chamber SIGMA at the 5 MV 15-SDH-2 tandem accelerator (Tandem laboratory) at Uppsala University (Sweden). The setup is equipped with Passivated Implanted Planar Silicon detectors (PIPS), a Silicon Drift Detector (SDD) and an e^--beam evaporator (FOCUS EFM 3T), enabling *in-situ* ion beam analysis (IBA) of thin films under deposition. A leak valve installed between the main chamber and a gas feed system allows different gas environments, whereas a large optical viewport is used to illuminate samples inside the chamber with light. For more details of the scattering chamber, we refer to literature [20].

A bilayer film consisting of an YH_2 layer on top of YHO was deposited onto a C substrate. The choice of the substrate allows the unambiguous identification of O in the thin films. Metallic Y (nominal purity: 99%) was evaporated in H_2 atmosphere ($P=3\times10^{-6}$ mbar) for 13 min. The resulting YH_2 layer turned photochromic upon exposure to air forming YHO. Films deposited at the same deposition conditions yielded photochromic films previously [9]. After oxidation, another YH_2 layer was grown onto the YHO film under identical conditions. The bilayer structure (YH_2/YHO) with a gradient in the anion concentration enables to study diffusion and anion mobility. For photodarkening we used a blue LED-array (λ=455 nm, $W_{flux}\approx500$ mWcm^{-2}) as employed in Ref. [9].

The chemical composition and depth distribution of elements and their isotopes were determined by Rutherford Backscattering Spectrometry (RBS) using 2 MeV $^4He^+$ after each synthesis step. The angle between the incident ions and the PIPS detector (i.e. scattering angle) was 170°. The normal of the sample surface was rotated 140° with respect to the direct beam. This geometry improves the depth resolution due to an increased path length of the probing ions in the film. Characteristic x-rays emitted under He irradiation were detected by the SDD. L_α x-rays of Y were used to normalize the RBS spectra. All RBS spectra were analyzed using SIMNRA [21].

2.2 *Ex-situ* analysis

After the *in-situ* experiments the samples were studied *ex-situ*. Time of Flight – Energy Elastic Recoil Detection Analysis (ToF-E ERDA) was used to quantify the depth distribution of all constituents. The ^{18}O content in the films was extracted from Nuclear Reaction Analysis (NRA) with enhanced depth resolution.

ToF-E ERDA measurements were carried out at the tandem accelerator using 36 MeV $^{127}I^{8+}$ as probing beam. Recoil species from the target were detected at a detection angle of 45° by a combined segmented anode gas ionization chamber and time-of-flight detector. More technical details on ToF-E can be found elsewhere [22]. The incident angle was 67.5°. Possible sources of systematic uncertainties of ERDA measurements were discussed in detail in Ref. [17]. Depth profiles of chemical elements were derived using Potku [23].

Profiling of ^{18}O was done at the single stage 350 kV Danfysik implanter (Tandem Laboratory, Uppsala University) using the $^{18}O(p,\alpha)^{15}N$ nuclear reaction and taking advantage of its sharp resonance at 151 keV (Γ_R = 100 eV). A depth profile is obtained by increasing the energy of incident protons stepwise starting from energies below the resonance. Alpha particles originating from the nuclear reaction are detected by a PIPS detector with large solid angle placed at 150° mean detection angle and covered by a 4 μm Al foil to avoid backscattered particles. The sample normal was 10° from the incident beam direction. For more details on instrumentation employed for NRA measurements we refer to Ref. [24].

3 Results and discussions

RBS measurements on the bilayer sample were conducted immediately after deposition and repeated 30 minutes later. In between the measurements, the sample was stored under high vacuum ($P \approx 5\times10^{-8}$mbar) conditions. Figure 1a) shows both RBS spectra normalized. The data were normalized using the substrate signal. Figure 1b) is a zoom into the energy region of the O signal. The vertical dashed grey line indicates the interface between the oxidised layer and the additional layer after deposition but before oxidation. The films (black open circles in Figure 1) contain uniformly distributed O at a level of 36 at. % in the bottom layer and up to 5 at. % of O in the top one. The oxygen impurity may be related to residual gas in the pipes used to inject H_2 during evaporation. The distribution of all chemical elements remains the same after 30 min (red crosses in Figure 1) apart from an O-enriched layer appearing right at the surface. A fit to the O peak at the surface yields 1.4×10^{16} at/cm^2 added oxygen atoms.

At a pressure of 5×10^{-8} mbar and a temperature of 22°C the particle flux of air is 1.42×10^{13} cm^{-2}s^{-1} [25]. The number of particles hitting the surface of the sample in 30 minutes is 2.5×10^{16} at/cm^2, which is in good agreement with the number extracted from the RBS measurement, assuming that most of the residual gas is oxygen, water or hydroxyl. We conclude that the residual gas in the chamber is the reason for the observed surface oxidation but no material transport between the layers in the film is detected.

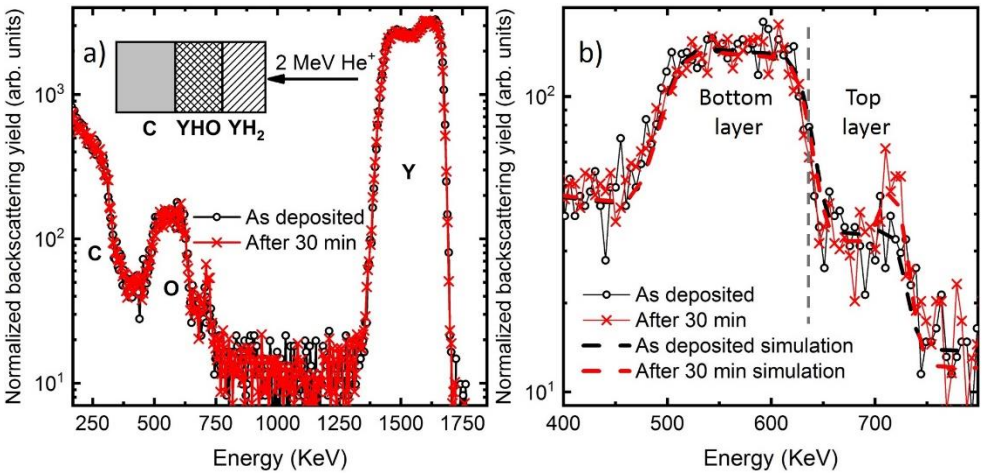

Fig. 1. RBS spectra (a) and zoom-in in the region associated with O signals (b) of the bilayer film taken as deposited (black open circles) and after 30 min in HV (red crosses). Black and red dashed lines show fit done using SIMNRA. The vertical dashed grey line indicates the interface between the two layers.

To study the oxidation process in more detail a second bilayer sample (YH_2/YHO) was grown but this time oxidized in $^{18}O_2$ (isotopically enriched to 97%) at a pressure of 3×10^{-3} mbar for 3 min and subsequently exposed to air. Figure 2a) shows the part of RBS spectra with the O-signal of the as-deposited film (black-open circles) and after oxidation in $^{18}O_2$ (red crosses) as well as after exposure to air (blue squares). The vertical dashed grey line indicates the interface between the two layers. Exposure to $^{18}O_2$ results in partial oxidation of the top layer with both ^{16}O and ^{18}O. The presence of ^{16}O is attributed to contamination of the gas feed system. Further exposure to air leads to continuous oxidation. Remarkably, the additional oxygen, which is predominantly ^{16}O does not replace ^{18}O nor redistributes it but rather further oxidizes the film throughout its full thickness. This fact supports the hypothesis that oxidation progresses along permeable grain boundaries and intercolumnar voids. Moreover, the result clearly shows that oxygen atoms are tightly bound once the oxide is formed. These results provide further evidence for the hypothesis of a two phase nature of the material with a columnar structure as found in GdHO films and revealed by transmission electron microscopy [19].

Films deposited at identical conditions on CaF_2 substrates show photochromic properties [9]. Therefore, it is plausible to assume that the films studied in this work are also transparent and photochromic, despite the opaque nature of the substrate obscuring the optical properties but allowing a detailed study of the oxygen inventory with RBS. A potential influence of illumination on material migration, oxygen diffusion, was investigated. RBS spectra recorded before and after 10 min of illumination and shown as black open circles and red crosses, respectively, are presented in Figure 2b). No detectable changes in chemical composition are observed, excluding light-induced oxygen transport over long distances but leaving a possibility of a local diffusion over distance smaller than the depth resolution, which is several 10's of nm.

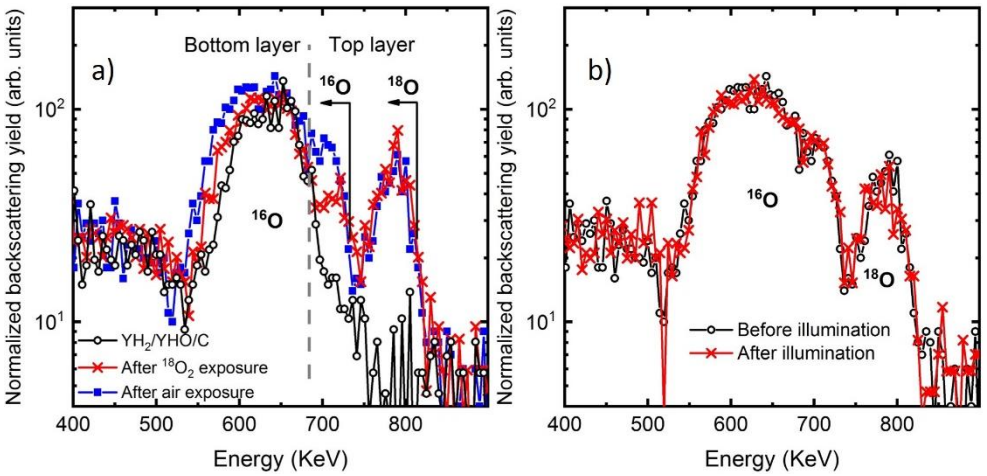

Fig. 2. Oxygen RBS signals of the bilayer film (a) recorded for the as deposited sample (black open circles), after exposure to $^{18}O_2$ of pressure 3×10^{-3} mbar for 3 min (red crosses) and oxidation in air (blue squares). Oxygen signals (b) before (black open circles) and after 10 min of illumination (red crosses).

The sample studied under illumination was characterized by ToF-E ERDA and NRA 4 days and 13 days after deposition. Figure 3a) shows that all chemical elements including O are uniformly distributed throughout the film despite of the fact that the sample was grown in two layers. The presence of C in the film (8-9 at. %) is explained by discontinuities in the film due to partial delamination over time. It is known that the stability of YHO films in air and produced by e$^-$-beam evaporation is lower as compared to the ones produced by magnetron sputtering [9]. Both ERDA and NRA (Figure 3a and 3b, respectively) confirm that ^{18}O is primarily concentrated in the top layer again suggesting progressive oxidation along grain boundaries not affecting existing oxidic domains.

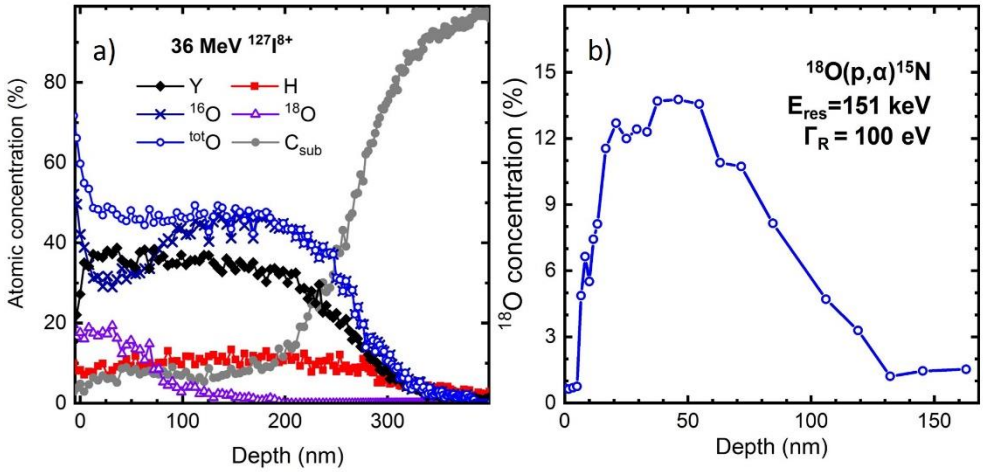

Fig. 3. Depth profile of chemical elements for the fully oxidized bilayer YHO film derived from ToF-E ERDA (a). Depth distribution of ^{18}O in the YHO film calculated from NRA measurements (b).

4 Summary and conclusions

We have prepared bilayer YH_2/YHO films and studied their oxidation and oxygen mobility by tracking the chemical composition using isotope-sensitive IBA. We show that a gradient in the anion concentration, artificially created in the film, persists over time, demonstrating low oxygen mobility. Using ^{18}O as a tracer, we conclude that oxidation of YH_2 progresses through grain boundaries and intercolumnar voids not effecting pre-existing O. The result implies that the oxidation rate may be controlled via the films microstructure. Composition analysis of isotope-labeled photochromic YHO film before and after illumination reveals no detectable changes. This proves that long-range diffusion of anions can not be responsible for photodarkening and supports the hypothesis of inter-phase H transfer, as proposed in Ref. [19].

The authors would like to thank the Swedish Research Council VR-RFI (contracts No. 2017-00646-9 and 2019-00191) and the Swedish Foundation for Strategic Research (contract RIF14-0053) for supporting accelerator operation. DM thanks the Swedish Institute for the stipend for his research visit at Uppsala University granted as part of the Visby program. CA acknowledges the ERASMUS+ Programme which supported her stay at Uppsala University.

References

[1] T. Ahmad and D. Zhang, Energy Reports, **6**, 1973–1991 (2020).

[2] T. Mongstad, C. Platzer-Björkman, J.P. Maehlen, L.P.A. Mooij, Y. Pivak, B. Dam, E.S. Marstein, B.C. Hauback, and S.Z. Karazhanov, Sol. Energy Mater. Sol. Cells, **95**, no. 12, 3596–3599 (2011).

[3] S. M. M. Aðalsteinsson, M. V. V Moro, D. Moldarev, S. Droulias, M. Wolff, and D. Primetzhofer, Nucl. Instruments Methods Phys. Res. Sect. B Beam Interact. with Mater. Atoms, **485**, 36–40 (2020).

[4] F. Nafezarefi, H. Schreuders, B. Dam, and S. Cornelius, Appl. Phys. Lett., **111**, no. 10, 103903 (2017).

[5] C. C. You, T. Mongstad, E. S. Marstein, and S. Z. Karazhanov, Materialia, **6**, no. April, 100307 (2019).

[6] T. He and J. N. Yao, Res. Chem. Intermed., **30**, no. 4–5, 459–488 (2004).

[7] A. B. A. Kayani S. Kuriakose, M. Monshipouri, F.A. Khalid, S. Walia, S. Sriram, and M. Bhaskaran, Small, **17**, no. 32, 2100621 (2021).

[8] J. Montero, F. A. Martinsen, M. Lelis, S. Z. Karazhanov, B. C. Hauback, and E. S. Marstein, Sol. Energy Mater. Sol. Cells, **177**, 106–109 (2018).

[9] K. Kantre, M. V. Moro, D. Moldarev, M. Wolff, and D. Primetzhofer, Scripta Materialia, **186**. 352–356 (2020).

[10] C. C. You, D. Moldarev, T. Mongstad, D. Primetzhofer, M. Wolff, E.S. Marstein, and S.Z. Karazhanov, Sol. Energy Mater. Sol. Cells, **166** (2017).

[11] D. Moldarev, M. V Moro, C.C. You, E.M. Baba, S.Z. Karazhanov, M. Wolff, and D. Primetzhofer, Phys. Rev. Mater., **2**, no. 11, 115203 (2018).

[12] J. P. Maehlen, T. T. Mongstad, C. C. You, and S. Karazhanov, J. Alloys Compd., **580**, S119–S121 (2013).

[13] M. P. Plokker, S.W.H. Eijt, F. Naziris, H. Schut, F. Nafezarefi, H. Schreuders, S. Cornelius, and B. Dam, Sol. Energy Mater. Sol. Cells, **177**, no. March 2017, 97–

105 (2018).

[14] D. Chaykina, T. de Krom, G. Colombi, H. Schreuders, A. Suter, T. Prokscha, B. Dam, and S. Eijt, Phys. Rev. B, **103**, no. 22, 224106 (2021).

[15] E. M. Baba, J. Montero, E. Strugovshchikov, E. Ö. Zayim, and S. Karazhanov, Phys. Rev. Mater., **4**, no. 2, 1–8 (2020).

[16] D. Moldarev, L. Stolz, M. V Moro, S.M. Aðalsteinsson, I.-A. Chioar, S.Z. Karazhanov, D. Primetzhofer, and M. Wolff, J. Appl. Phys., **129**, no. 15, 153101 (2021).

[17] M. V Moro, D. Moldarev, C.C. You, E.M. Baba, S.Z. Karazhanov, M. Wolff, and D. Primetzhofer, Sol. Energy Mater. Sol. Cells, **201**, 110119 (2019).

[18] M. V Moro, S.M. Aðalsteinsson, T.T. Tran, D. Moldarev, A. Samanta, M. Wolff, and D. Primetzhofer, Phys. status solidi – Rapid Res. Lett., vol. 15, no. 6, p. 2000608, Jun. 2021.

[19] M. Hans, T.T. Tran, S.M. Aðalsteinsson, D. Moldarev, M. V. Moro, M. Wolff, and D. Primetzhofer, Adv. Opt. Mater., **2000822**, 1–6 (2020).

[20] K. Kantre, M.V. Moro, D. Moldarev, D. Johansson, D. Wessman, M. Wolff, and D. Primetzhofer, Nucl. Instruments Methods Phys. Res. Sect. B Beam Interact. with Mater. Atoms, **463** (2020).

[21] M. Mayer, W. Eckstein, H. Langhuth, F. Schiettekatte, and U. Von Toussaint, Nucl. Instruments Methods Phys. Res. Sect. B Beam Interact. with Mater. Atoms, **269**, no. 24, 3006–3013 (2011).

[22] P. Ström, P. Petersson, M. Rubel, and G. Possnert, Rev. Sci. Instrum., **87**, no. 10, 103303 (2016).

[23] K. Arstila, J. Julin, M.I. Laitinen, J. Aalto, T. Konu, S. Kärkkäinen, S. Rahkonen, M. Raunio, J. Itkonen, J.-P. Santanen, T. Tuovinen, and T. Sajavaara, Nucl. Instruments Methods Phys. Res. Sect. B Beam Interact. with Mater. Atoms, **331**, 34–41 (2014).

[24] S. A. Corrêa, E. Pitthan, M. V Moro, and D. Primetzhofer, Nucl. Instruments Methods Phys. Res. Sect. B Beam Interact. with Mater. Atoms, **478**, 104–110 (2020).

[25] J. F. O'Hanlon, "Gas Properties," A User's Guide to Vacuum Technology, 9–24 (2003).